ELECTRON-PHONON INTERACTION IN FLUORIDE CRYSTALS DOPED WITH ISOELECTRONIC $3d^3$ IONS $(V^{2+}, Cr^{3+}, Mn^{4+})$

N. M. AVRAM[1], M. G. BRIK[2], C. N. AVRAM[1]

[1] *Department of Physics, West University of Timisoara,*
Bd. V. Parvan Nr. 4, 300223 - Timisoara, Romania
[2] *Institute of Physics, University of Tartu, Riia Street 142, 51014 Tartu, Estonia*
E-mail: avram@physics.uvt.ro

Abstract. The aim of this paper is to investigate the electron-phonon coupling between optical electrons of the V^{2+}, Cr^{3+} and Mn^{4+} ions doped in fluoride crystals $CsCaF_3$:V^{2+}, $KMgF_3$:Cr^{3+}, $LiCaAlF_6$:Cr^{3+}, and Cs_2GeF_6:Mn^{4+}. The $^4T_{2g}$ spinor splitting of these ions, due to spin-orbit interaction has been modeled by the second order spin-orbit Hamiltonian. Effect of the dynamical Jahn-Teller interaction on the spin – orbit splitting of $^4T_{2g}$ term is taken into account and the Jahn-Teller stabilization energy, zero-phonon line splitting and Huang-Rhys parameter are evaluated.

The position of the potential surfaces of the $^4T_{2g}$ excited state is considered using an analysis of the displacements of ligands due to the combined effect of the a_{1g} and e_g normal modes of the octahedral complex forming by the considered impurities and nearest environment. The net result of these vibrations, both axial and equatorial was obtained. The comparison with experimental data is discussed.

Key words: transition metal ions, fluoride crystals; electron-phonon interaction; Jahn-Teller stabilization energy.

1. INTRODUCTION

Transition metal ions as the optical active centers in various crystals have been the subject of a great number of experimental and theoretical studies (*e.g.* [1, 2] and references therein). Electronic transitions between the energy levels of their external unfilled $3d$ shell give rise to the intense and broad (or sharp) luminescence bands depending on the spin and symmetry of the states involved into the transitions and the dynamic of the environment surrounding the active ions in crystal.

The host materials doped with transitional metal ions with $3d^3$ electron configuration (V^{2+}, Cr^{3+} and Mn^{4+}) have received considerable attention, both experimental and theoretical, during the development of the crystal and ligand field

theories [3–6]. The reason is that the $3d^3$ electron shell has a very attractive combination of the spin-doublet and spin-quartet states in the octahedral crystal field, which allows for getting either sharp luminescence lines (in the case of a strong crystal field, when the first excited state is the ^2E_g doublet) or broadband luminescence (in the case of a weak crystal field with the $^4T_{2g}$ quartet being the first excited state). Among different possible hosts for these ions, fluoride crystals are especially interesting from the spectroscopic point of view, since the phonon cut-off energy is rather low causing the emission life-time of the excited state to be greater, than, for example, in oxide crystals. For most fluoride crystals the impurity ions -V^{2+}, Cr^{3+} and Mn^{4+} have octahedral site symmetry.

In an octahedral ligand field the five fold-degenerate energy level of a 3d electron splits into a doubly degenerate level e_g, with additional energy +6 Dq and a triple degenerate level t_{2g} with additional energy –4 Dq (these energies are related to the non-split 3d state). Thus the energy-level splitting is 10 Dq, where Dq is the so called crystal field strength, which varies for different ions and crystals from about 1.000 cm^{-1} to 2.000 cm^{-1}.

For 3d- electron systems, the energies E_i of the $3d^n$ levels in an exact octahedral configuration of ligands are derived as the functions of the crystal-field strength Dq and of the Racah parameters B and C. In the so-called Tanabe-Sugano diagrams, E_i/B are depicted as function of Dq/B for a fixed value of C/B [7, 8]. In Fig. 1 a Tanabe-Sugano diagram for $3d^3$ ion [7] is shown.

The spectroscopic properties of the transition metal ions in the fluorides are characterized primarily by the absorption and emission band structures. Some relatively narrow line features may be superimposed on the broad absorption and emission bands. These transitions are referred to as the vibronic transitions because they involve the simultaneous absorption or emission of both photons and phonons.

All spectra of the V^{2+}, Cr^{3+} and Mn^{4+} ions in various fluoride crystals are strongly influenced by the static crystal field of the host matrix and coupling between the phonons of the host matrix and electronic state of the impurity ion.

The calculations of the fine structure of energy levels in $CsCaF_3$:V^{2+}, $KMgF_3$:Cr^{3+}, $LiCaAlF_6$:Cr^{3+}, and Cs_2GeF_6:Mn^{4+}, accompanied by estimations of the Jahn-Teller (JT) stabilization energy in the excited state $^4T_{2g}$ of impurity ions are presented in this paper. Two independent approaches – effective second-order spin-orbit Hamiltonian and analysis of the potential energy surfaces – are used. JT energy was estimated in the first and the second models, respectively, in the frame of crystal-field theory taken into account the vibronic-coupling effect. The above-mentioned fluoride crystals have a structure that can accommodate a substitutional trivalent cation impurity in a site of rigorous octahedral symmetry without charge compensation. The electronic states of interest are the $^4A_{2g}$ and $^4T_{2g}$ states, all derived from the free-ion $3d^3$ ground configuration of V^{2+}, Cr^{3+} and Mn^{4+} ions, as indicated by the Tanabe-Sugano diagram shown in Fig. 1; all these states have the same parity.

Fig. 1 – Tanabe-Sugano diagram for a
$3d^3$-ion in an octahedral crystal field [7].
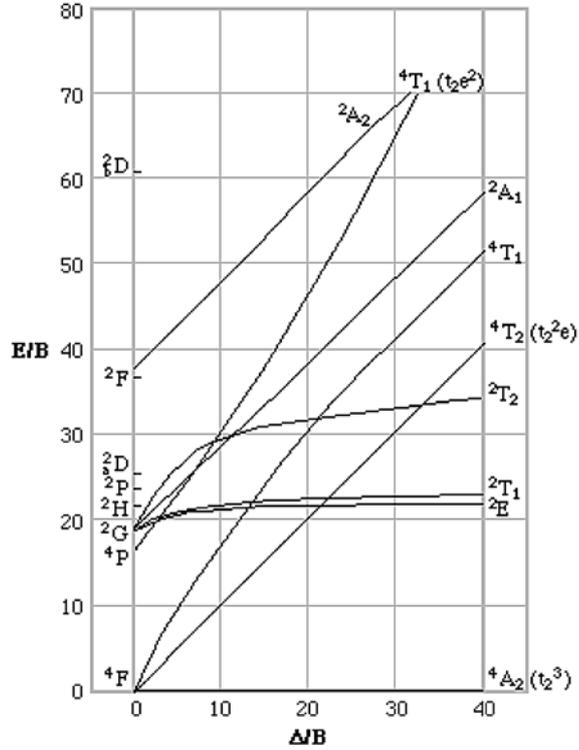
2. PARAMETERS OF THE ELECTRON-PHONON INTERACTION

The main approximation of the crystal-field theory (which, initially, took into account the Coulomb interaction between the central ion and ligands only, without considering an electron structure of ligands) is associated with the introduction of the effective Hamiltonian of the dopant ion with an unfilled d electron shell

$$H = H_0 + V_{cr} + V_{ee} + V_{so} + V_{\text{e-p}}, \tag{1}$$

where H_0 is the Hamiltonian of a free ion, V_{cr} is the ion interaction with lattice, V_{ee} is the energy of the electrostatic interaction of the activator electrons, V_{so} is the operator of the spin-orbit interaction and $V_{\text{e-p}}$ describes the electron-phonon interaction. In order to find the energy levels of every electronic configuration, it is necessary to calculate the eigenvalues of the operator H, taking into account the relative order of magnitude of different terms in Hamiltonian (1) and using perturbation theory.

To study electron-phonon coupling of the V^{2+}, Cr^{3+} and Mn^{4+} ions with the lattice vibrations of considered crystals, we used the single configurational coordinate

model in harmonic approximation [9]. This model is based on the assumption that the nearest environment of the impurity ion oscillates harmonically about its equilibrium position. This displacement is described by the Q coordinate. A typical diagram of the potential energies of electronic states as a function of the vibrational coordinate Q for the case of a strong crystal field (when the orbital doublet ^2E is located below the orbital triplet $^4T_{2g}$) is sketched in Fig. 2.

Two main parameters which describe the electron-phonon coupling are the Huang-Rhys parameter S and the effective phonon energy $\hbar\omega$. The former is defined as the number of phonons of the energy $\hbar\omega$ excited in the absorption transition [9]:

$$S = \frac{E_{dis}}{\hbar\omega},\qquad(2)$$

where E_{dis} is defined in Fig. 2. Both parameters S and $\hbar\omega$ are related to the difference between the first absorption and corresponding emission bands peaks
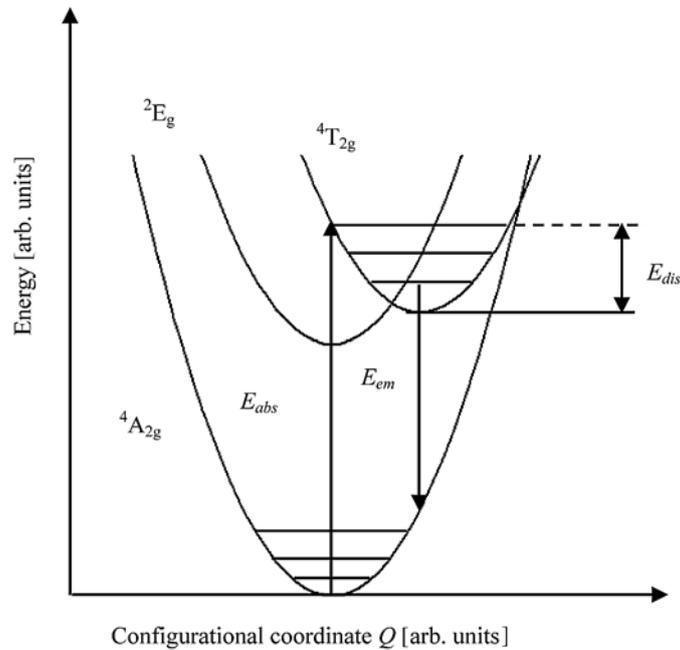

Fig. 2 – Single configurational coordinate diagram for LiCaAlF$_6$:Cr^{3+} (schematic representation). The lowest electronic states are shown; the vibrational frequencies in all electronic states are assumed to be the same. Vibrational energy levels are indicated by horizontal lines. Absorption and emission transitions are indicated by the up-ward and down-ward arrows, respectively. The difference between the excited state vibrational level reached in the absorption transition and the minimum of the same parabola is denoted by E_{dis}.

(Stokes shift) ΔE by the following expression [9–10]:

$$\Delta E = \left(2S - 1\right)\hbar\omega. \tag{3}$$

The second equation which is required for calculate the values of S and $\hbar\omega$ is as follows [9, 10]:

$$\Gamma(T) = 2.35\hbar\omega\sqrt{S\coth\left(\frac{\hbar\omega}{2kT}\right)}, \tag{4}$$

where $\Gamma(T)$ is the full width at half maximum (FWHM) at the absolute temperature T. The Stokes shift ΔE between the maxima of the $^4A_{2g} - {}^4T_{2g}$ absorption and corresponding $^4T_{2g} - {}^4A_{2g}$ emission, and the FWHM of the $^4T_{2g} - {}^4A_{2g}$ emission band are obtained experimentally. Solving equations (2)–(3) yields the values of both parameters S and $\hbar\omega$.

The obtained results for the Stokes shifts S and $\hbar\omega$ energy, will be used for the analysis of the JT effect.

3. HAM EFFECT IN THE $^4T_{2G}$ STATE: THE $T \otimes e$ INTERACTION IN CsCaF₃:V²⁺, KMgF₃:CR³⁺, LiCaAlF₆:Cr³⁺, AND Cs₂GeF₆:Mn⁴⁺

Due to an interaction between optical electrons of an impurity ion and JT active vibrational modes, the observed spin-orbit (SO) splitting of the orbital triplet states is reduced several times in magnitude, compared to the splitting which is expected to be from the theoretical calculations. This is known as the Ham effect [11], and serves as a firm experimental evidence of the JT effect. Comparison of the experimental and calculated SO splittings of the orbital triplets gives a possibility of the direct evaluation of the JT stabilization energy E_{JT} for the considered complex. It is convenient to express the calculated SO splittings in terms of the dimensionless parameter (Ham reduction factor)

$$\gamma = \exp\left(-\frac{3E_{JT}}{2\hbar\omega}\right), \tag{5}$$

where $\hbar\omega$ stands for the energy of the JT active mode (which here and thereafter is assumed to be the e_g normal mode; it interacts more strongly with the electronic states than other normal modes of the octahedral complex). Below the case of CsCaF₃:V²⁺ [12] is given in more details.

Numerical diagonalization of Hamiltonian (1), neglecting the last term, for d³ configuration, allows to get the fine structure of the V²⁺ energy levels. The SO constant was chosen to be equal to 136 cm⁻¹. In the octahedral double group the twelve–fold degenerated $^4T_{2g}$ term is split by the SO interaction into four sublevels:

$$^4T_{2g} \rightarrow \Gamma_6 + \Gamma_7 + \Gamma_8^a + \Gamma_8^b \qquad (6)$$

Their calculated energies (compared to the experimentally observed splitting) are shown in Table 1.

Table 1

Fine structure of $^4T_{2g}$ level in CsCaF$_3$:V^{2+}

Γ	Theory	Exp.	Jahn-Teller effect
Γ_7	0	0	0
Γ_8^a	32	9	13.8
Γ_8^b	77	20	20.6
Γ_6	89	31	27.9

To model the observed spin-orbit splitting an effective second order spin-orbit Hamiltonian [13–15] is used:

$$H_{eff} = \lambda \vec{L} \cdot \vec{S} + k(\vec{L} \cdot \vec{S})^2 + \rho(L_x^2 S_x^2 + L_y^2 S_y^2 + L_z^2 S_z^2), \qquad (7)$$

operating in the space of twelve wave functions of $^4T_{2g}$ degenerated state with $L = 1$ and $S = 3/2$. The $^4T_{2g}$ basis functions for the matrix of H_{eff} are $|iM_s\rangle$, with the orbital functions i transforming as ξ, η, ζ orbitals and $M_s = 3/2, 1/2, -1/2, -3/2$. The values of parameters λ, κ, and ρ are determined by fitting the eingenvalues of the H_{eff} matrix to the $^4T_{2g}$ spinor splitting calculated with the full d^3 matrices. The obtained values are: $\lambda = 21$ cm^{-1}, $\kappa = 2.2$ cm^{-1} and $\rho = -6.9$ cm^{-1}.

Now the electron-phonon interaction term in Hamiltonian (1) is considered. The [VF$_6$]$^{4-}$ cluster is an octahedron and has one e_g and one t_{2g} JT active normal modes. The former is typically expected to interact more strongly with the electronic states of an octahedral coordinated impurity ion than the latter. The linear JT Hamiltonian corresponding to the interaction of electronic $^4T_{2g}$ state with e_g vibration is (without taking into account the "harmonic" part)

$$H_{JT} = -V \begin{bmatrix} -\dfrac{1}{2}Q_\theta + \dfrac{\sqrt{3}}{2}Q_\varepsilon & 0 & 0 \\ 0 & -\dfrac{1}{2}Q_\theta - \dfrac{\sqrt{3}}{2}Q_\varepsilon & 0 \\ 0 & 0 & Q_\theta \end{bmatrix}, \qquad (8)$$

where V is the coupling constant, $Q_\theta(\sim x^2 - y^2)$ and $Q_\varepsilon(\sim 3z^2 - r^2)$ are the collective coordinates of the e_g mode. Using the Born–Oppenheimer approximation,

one can factorize the matrix elements of vibronic wave functions into pure electronic and vibrational parts, respectively:

$$\langle i, M_s, n_\theta, n_\varepsilon | H_{eff} | j, M_s', n_\theta', n_\varepsilon' \rangle =$$
$$= \langle i, M_s | H_{eff} | j, M_s' \rangle \langle i, M_s, n_\theta | j, M_s', n_\theta' \rangle \langle i, M_s, n_\varepsilon | j, M_s', n_\varepsilon' \rangle, \qquad (9)$$

where n_θ, n_ε represent the number of vibrational quanta of the θ and ε component of the e_g mode. Considering only the ground vibrational states, $n_\theta = n_\varepsilon = 0$ and assuming harmonic potentials, the last equation can be rewritten as

$$\langle i, M_s, 0, 0 | H_{eff} | j, M_s', 0, 0 \rangle = \langle i, M_s | H_{eff} | j, M_s' \rangle [\delta_{ij} + \gamma(1 - \delta_{ij})]. \qquad (10)$$

The observed experimental $^4T_{2g}$ spinor splitting can be fitted with H_{eff} matrix including the Ham reduction factor γ by keeping the above determined values of
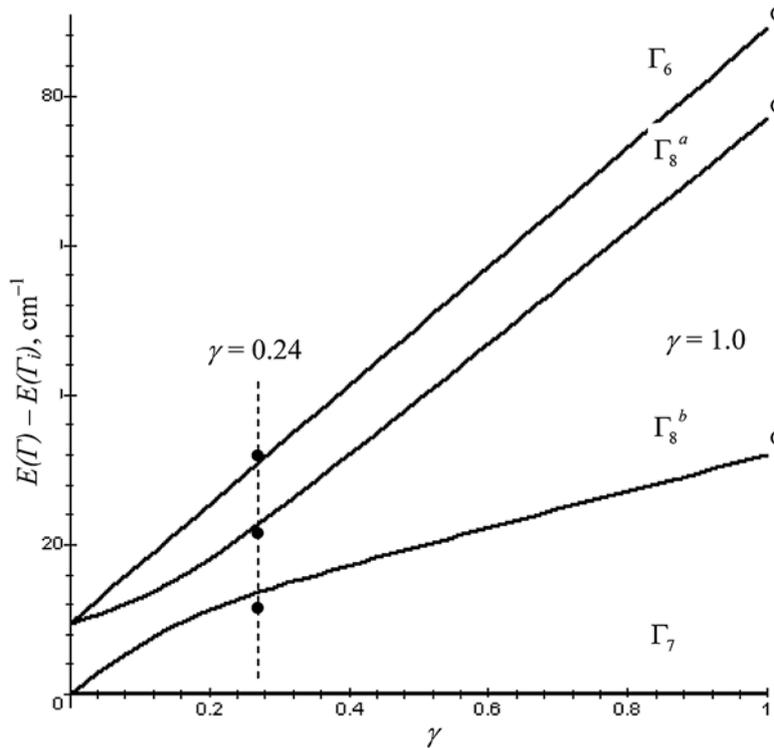

Fig. 3 – The Ham effect in the $^4T_{2g}$ term of CsCaF$_3$:V^{2+} [12]. The curves are the splitting as functions of the Ham reduction factor γ calculated from the first order Ham theory. The empty circles correspond to the energy of spinors in static crystal field ($\gamma = 1.0$), the filled circles are the experimental energies.

parameters λ, k and ρ fixed and letting only γ to vary. The results are given in Table 1, column c, and in Fig. 3.

Since the Ham reduction factor γ is directly related to the JT stabilization energy E_{JT}, we estimated this energy value taking for e_g vibrations $\hbar\omega_{JT} = 388$ cm^{-1} [16] to be $E_{JT} = 369$ cm^{-1} which corresponds to $\gamma = 0.24$. In case $\gamma = 0$ (strong JT coupling) four spinors merge into two six-fold degenerated states, separated by $2(k + \rho) = 9.4$ cm^{-1} (ZPL splitting). After E_{JT} is found, the value of Huang-Rhys parameter S can be readily estimated as $S = 0.95$, close to that one (0.87) estimated for isoelectronic Cr^{3+} embedded into isostructural crystal KMnF$_3$ [15]. Similar results have been obtained for KMgF$_3$:Cr^{3+} [17], LiCaAlF$_6$:Cr^{3+}[18] and Cs$_2$GeF$_6$:Mn^{4+} [19](see also [20–23]).

4. GEOMETRY OF THE ^{4}T$_{2g}$ EXCITED STATE IN CsCaF$_3$:V^{2+}, KMgF$_3$:Cr^{3+} , LiCaAlF$_6$:Cr^{3+}, AND Cs$_2$GeF$_6$:Mn^{4+}

The adiabatic potentials corresponding to the ground and excited states of V^{2+}, Cr^{3+} and Mn^{4+} ions in the octahedral complexes of the considered crystals have different geometries. This leads to a relative displacement of their potential energy surface along the a_{1g} and e_g normal modes of cluster. In order to calculate the equilibrium displacements of the ^{4}T$_{2g}$ from the ground state along the a_{1g} and e_g active modes the following equation [9] can be used:

$$\left| \Delta Q_i \right|_{eq} = \left[\frac{2 S_i h \nu_i}{f_i} \right]^{1/2} . \tag{11}$$

Here Q_i denotes the ith normal mode of the formed cluster, with the force constant f_i of harmonic potential; S_i are the Huang – Rhys factors.

The f_i constants were calculated with the FG matrix method for an octahedral cluster and experimental values for $h\nu_{a_{1g}}$ and $h\nu_{e_g}$. The Huang-Rhys factor S_{e_g} will be calculated based on the Ham quenching of the ^{4}T$_{2g}$ spin–orbit splitting due to the dynamical JT effect.

The values of $\left| \Delta Q_{a_{1g}} \right|_{eq}$ and $\left| \Delta Q_{e_g} \right|_{eq}$ can be estimated from Eq. (11). It was shown that $\Delta Q_{a_{1g}eq}$ is positive, whereas ΔQ_{e_geq} is negative.

The coordinate system in the $(Q_\theta, Q_\varepsilon)$ space can always be chosen in such a way, that the potential minimum of the ^{4}T$_{2g}$ component under consideration (either ξ, η or ζ) lies on the Q_θ axis, i.e. no distortion occurs along Q_ε. Then it is possible

to consider the $\left.\left|\Delta Q_{e_g}\right|\right._{eq}$ values as corresponding to $\left.\left|\Delta Q_{e_g\theta}\right|\right._{eq}$, whereas $\left.\left|\Delta Q_{e_g\varepsilon}\right|\right._{eq}$ is zero. Also, we will use the connection between displacements of normal coordinates ΔQ and the changes in the metal-ligand bond lengths

$$\begin{pmatrix} \Delta x \\ \Delta y \\ \Delta z \end{pmatrix} = \frac{1}{2} \begin{pmatrix} \sqrt{\dfrac{2}{3}} & -\sqrt{\dfrac{1}{3}} & -1 \\ \sqrt{\dfrac{2}{3}} & -\sqrt{\dfrac{1}{3}} & 1 \\ \sqrt{\dfrac{2}{3}} & \sqrt{\dfrac{4}{3}} & 0 \end{pmatrix} \begin{pmatrix} \Delta Q_{a_{1g}} \\ \Delta Q_{e_g\theta} \\ \Delta Q_{e_g\varepsilon} \end{pmatrix}. \tag{12}$$

Eq. (12) explains why it is convenient to make a specific rotation of the coordinate system in the $(Q_\theta, Q_\varepsilon)$ space described above: if $\left.\left|\Delta Q_{e_g\varepsilon}\right|\right._{eq} = 0$, then $\Delta x = \Delta y$, and the potential energy surface can be easily visualized and the JT energy is obtained.

Table 2 contains the Huang-Rhys factors and equilibrium geometries of the $[MnF_6]^{2-}$ octahedron in the $^4T_{2g}$ first quartet excited state relative to the $^4A_{2g}$ ground state in the Mn^{4+} doped Cs_2GeF_6 crystal [19].

Table 2

Huang-Rhys factors and equilibrium geometries of the $[MnF_6]^{2-}$ octahedron in the $^4T_{2g}$
quartet excited state relative to the $^4A_{2g}$ ground state in Mn^{4+} doped Cs_2GeF_6

$S_{a_{1g}}$ 2.7 [24]	$\left.\left|\Delta Q_{a_{1g}}\right|\right._{eq}$ (Å) 0.16	$\Delta x_{eq}, \Delta y_{eq}$, (Å) 0.09
S_{e_g} 0.89 [19]	$\left.\left|\Delta Q_{e_g}\right|\right._{eq}$ (Å) −0.09	Δz_{eq} (Å) 0.01

The JT energy obtained from potential energy surface is 438 cm^{-1}.
The results of methods presented above are given below:
$CsCaF_3:V^{2+}$ (1), $KMgF_3:Cr^{3+}$ (2), $LiCaAlF_6:Cr^{3+}$ (3), and $Cs_2GeF_6:Mn^{4+}$ (4)

	1	2	3	4
Crystal field strength [cm^{-1}]	866	1450	1476	2063
Distance to the nearest ligand, [Å]	2.23	1.995	1.8	1.76
The first excited state	$^4T_{2g}$	$^4T_{2g}$	^2E_g	^2E_g
Dq/B ratio	1.5	1.91	2.15	4.2
Stokes shift	5.0	2.13	4.20	3.64
Ham reduction factor	0.24	0.31	0.15	0.26
JT energy [cm^{-1}, Ham effect]	369.0	356.7	579.0	438.0
JT energy [cm^{-1}, exc. st. geom.]	368.6	356.6	577.0	439.6

5. CONCLUSIONS

In this paper we have analyzed the electron-phonon interaction for isoelectronic $3d^3$-ions V^{2+},Cr^{3+} and Mn^{4+} in fluoride host matrix $CsCaF_3$, $KMgF_3$, $LiCaAlF_6$, and Cs_2GeF_6. The calculations of the fine structure of energy levels is accompanied by estimations of the JT stabilization energy in the excited state $^4T_{2g}$ of impurity ions using two independent approaches – effective second-order spin-orbit Hamiltonian and analysis of the potential energy surfaces of excited state. JT energy was estimated, in the frame of crystal-field theory, taking into account the vibronic-coupling effect between electronic state of the impurity ions and phonon of the host matrix.

The $^4T_{2g}$ excited state is dynamically distorted due to the JT interaction with the normal vibrations of the host lattice. The combined coupling of the $^4T_{2g}$ electronic state of the ions to the a_{1g} and e_g normal modes of lattices leads to distortion of the equilibrium geometry in the $^4T_{2g}$ state. These distortions are calculated. From the contour plot of the potential energy surface of the excited state, also the JT energy was estimated. Finally the results of both approaches were compared.

REFERENCES

1. R. C. Powell, *Physics of Solid-State Laser Materials*, Springer, Berlin, 1998.
2. S. Kück, Appl. Phys. B, **72**, 515 (2001).
3. S. Sugano, Y. Tanabe, H. Kamimura, *Multiplets of Transition-Metal Ions in Crystals*, Academic Press, New York, 1970.
4. I. B. Bersuker, *Electronic Structure and Properties of Transition Metal Compounds. Introduction to the Theory*, Wiley, New York, 1996.
5. N. P. Barnes, in *Tunable Lasers Handbook*, Ed. F. J. Duarte, Academic Press, New York, 1995, p. 219.
6. B. Henderson, R. H. Bartram, *Crystal-Field Engineering of Solid-State Laser Materials*, Cambridge University Press, Cambridge, 2000.
7. Y. Tanabe, S. Sugano, J. Phys. Soc. Jap., **9**, 766 (1954).
8. S. Sugano, Y. Tanabe, H. Kamimura, *Multiplets of Transitional-Metal Ions in Crystals*, Academic, New York, 1970.
9. B. Henderson, G. F. Imbush, *Optical Spectroscopy of Inorganic Solids*, Clarendon, Oxford, 1989, 645 pg.
10. D. J. Newman, B. Ng (Editors), *Crystal Field Handbook,* Cambridge, 2000.
11. F. S. Ham, Phys. Rev., **138**, A1727(1965).
12. C. N. Avram, M. G. Brik, J. Lumin., **108**, 319 (2004).
13. P. Koidl, Phys. Stat. Sol. (b), **74**, 477 (1976).
14. O. S. Wenger, H. U. Güdel, J. Chem. Phys., **114**, 5832 (2001).
15. M. D. Sturge, Phys. Rev., **B 1**, 1005 (1970).
16. S. López-Moraza, Z. Barandiarán. J.Chem. Phys., **105**, 50 (1996).
17. M. G. Brik, N. M. Avram, I. Tanaka, Phys. Stat. Sol. (b), **241(13)**, 2982 (2004).

18. C. N. Avram, M. G. Brik, J. Lumin., **102–103**, 81 (2004).
19. N. M. Avram, M. G. Brik, Z. Naturforsch., **60a**, *1*, 54 (2005).
20. N. M. Avram, M. G. Brik, J. Mol. Struct., **838**, *1–3*, 198 (2007).
21. M. G. Brik, N. M. Avram, J. Mol. Struct., **838**, 193–197 (2007).
22. C. N. Avram, M. G. Brik, N. M. Avram, J. Lumin., **doi.10.1016/j.lumin.2007.10.038**.
23. A. Reisz, C. N. Avram, Acta Physica Polonica A, **112(5)**, 829 (2007).
24. L. Seijo, Z. Barandiaran, D. S. McClure, Int. J. Quantum Chem., **80** (2000) 623.